Available online at www.sciencedirect.com
SCIENCE DIRECT®
Journal of Sound and Vibration 279 (2005) 345–371
JOURNAL OF SOUND AND VIBRATION
www.elsevier.com/locate/jsvi

An efficient coupled zigzag theory for dynamic analysis of piezoelectric composite and sandwich beams with damping

S. Kapuria*, A. Ahmed, P.C. Dumir

Department of Applied Mechanics, Indian Institute of Technology, IIT Delhi, Hauz Khas, New Delhi 110016, India

Received 19 February 2003; accepted 6 November 2003

Abstract

An efficient new coupled zigzag theory is developed for dynamics of piezoelectric composite and sandwich beams with damping. Third order zigzag approximation is used for the axial displacement. The electric field is approximated as piecewise linear for the sublayers. The conditions of zero transverse shear stress at the top and bottom and its continuity at the layer interfaces, are *for the first time enforced exactly* in this theory. Using these conditions, the displacement field is expressed in terms of three primary displacement variables and potentials. The governing equations are derived from Hamilton's principle. Analytical solutions of simply-supported beams are obtained for natural frequencies and steady state forced response under harmonic electromechanical load with damping. These are compared with the exact two-dimensional piezoelasticity solution and the uncoupled first order shear deformation theory (FSDT) solution. The new results of forced damped response are more accurate than the FSDT solution and agree very well with the exact solution for both thin and thick hybrid beams. The developed theory adequately models open and closed circuit electric boundary conditions to accurately predict the response.

1. Introduction

Piezoelectric hybrid laminates with embedded or surface-bonded piezoelectric layers, acting as sensors and actuators to achieve desired control, form part of a new generation of adaptive structures. To achieve these objectives, robust coupled electromechanical models are needed to obtain accurate response of these hybrid structures. This work presents a new zigzag model for dynamic analysis of hybrid beams with embedded or surface-bonded piezoelectric layers. A review of three-dimensional (3-D) continuum-based approaches, 2-D theories for plates and shells and

*Corresponding author. Tel.: +91-1126591218; fax: +91-1126581119.
E-mail address: kapuria@am.iitd.ac.in, kapuria@am.iitd.ernet.in (S. Kapuria).

0022-460X/$ - see front matter © 2003 Elsevier Ltd. All rights reserved.
doi:10.1016/j.jsv.2003.11.018

1-D theories for beams, along with their comparative study for plates under static loading, has been presented by Saravanos and Heyliger [1]. Analytical 2-D solutions for free vibration [2] and harmonic forced response [3] are available only for simply-supported infinite flat panels and beams. The 3-D finite element analysis [4] results in large problem size which may become computationally costly for practical dynamics and control problems. Hence, accurate 1-D beam models are required without too much loss of accuracy compared to the 2-D models. Early works employed elastic beam models [5–7] with effective forces and moments due to induced strain of actuators. A discrete layer theory (DLT) with layerwise approximation of displacements was developed for elastic laminated beams with induced actuation strain by Robbins and Reddy [8]. Classical laminate theory (CLT) [9], first order shear deformation theory (FSDT) [10] and the refined third order theory (TOT) [11,12] have been applied without electromechanical coupling to hybrid beams and plates. Coupled CLT, FSDT and TOT [13–17] solutions have been reported for piezoelectric composite beams and plates including the charge equation of electrostatics and electromechanical coupling. Saravanos and Heyliger [18] have presented coupled DLT using layerwise approximation for displacement and potential, which yields very accurate results for thin and thick beams. But it is expensive for practical problems since the number of displacement unknowns depend on the number of sublayers. Except for the coupled DLT [18], in which the deflection w is taken as piecewise linear, no other theory described above includes the transverse normal strain induced through the piezoelectric coefficient d_{33}. This strain has considerable effect on the response for electrical load [1]. Kapuria [19] and Kapuria et al. [20] presented a coupled layerwise theory, for static and dynamic analysis of hybrid beams, using a third order zigzag approximation for the axial displacement u with a sublayerwise linear approximation for the potential ϕ. The deflection w is approximated to account for the piezoelectric transverse normal strain induced by the electric potential. The model considers both the axial and transverse electric fields. The conditions of zero shear stress τ_{zx} at the top and bottom surfaces and the conditions of continuity of τ_{zx} at the layer interfaces are *approximately satisfied* by neglecting the explicit contribution of ϕ. The theory is formulated in terms of only three primary displacement unknowns. It is as efficient as an equivalent single layer (ESL) theory and yet yields fairly accurate through-the-thickness variations of displacements, electric field and stresses. This theory has been recently improved [21] for static analysis using similar approximations for u, w, ϕ as in Ref. [20], but the conditions on τ_{zx} at the top, bottom and the layer interfaces are *exactly satisfied*. The coupled theory includes the cases wherein piezoelectric layers may be bonded to the surface of the elastic substrate or embedded in it. This theory has yielded accurate results for a test beam, a sandwich beam and a piezoelectric bimorph.

The statics theory of Ref. [21] is extended herein to dynamics. The coupled dynamic field equations and the variationally consistent boundary conditions are derived using the Hamilton's principle. The accuracy of the theory in estimating local and global dynamic response is assessed for simply-supported hybrid beams. The undamped natural frequencies and steady state forced damped response of the zigzag theory are compared with the exact 2-D piezoelasticity solution and the uncoupled FSDT solution. The effects of the ratio of span-to-thickness on the accuracy of the theory is investigated for a highly inhomogeneous test beam, a hybrid composite beam and a hybrid sandwich beam. The present theory yields highly accurate results for free and forced response of thin, moderately thick and even thick beams. Accurate results are obtained for open circuit as well as closed circuit electric conditions.

2. Formulation of zigzag theory for beams

Consider a hybrid beam (Fig. 1) of width b, thickness h and length a, made of L perfectly bonded orthotropic layers with longitudinal axis x, subjected to transverse load on the bottom and the top surfaces. The actuation potentials are applied to some piezoelectric layers. The loads have no variation along the width b. The axis along the width is y. The piezoelectric layers have poling along the thickness axis z. The sensors and actuators, considered herein, are of orthorhombic materials of class mm2 symmetry [22], since the commonly used materials PZT and PVDF belong to this class. The material of the piezoelectric layers can be different. The midplane of the beam is chosen as the xy plane with $z = z_0 = -h/2$ and $z = z_L = h/2$ being the bottom and the top surfaces of the beam. The z co-ordinate of the bottom surface of the kth layer (numbered from the bottom) is denoted as z_{k-1} and its material symmetry direction 1 is at an angle θ_k to the x-axis. The reference plane $z = 0$ either passes through or is the bottom surface of the k_0th layer. For a beam with a small width, the usual assumptions for mathematical simplification of the 1-D model made by other researchers which are retained in the present theory are: assume plane state of stress ($\sigma_y = \tau_{yz} = \tau_{xy} = 0$), neglect transverse normal stress ($\sigma_z \simeq 0$) and assume the axial and transverse displacements u, w and electric potential ϕ to be independent of y. In the classical theory σ_z is neglected. Exact elasticity solutions for thick beams and plates [23] have revealed that the contribution of σ_z to the strain energy is much smaller compared to that of τ_{zx}. Hence, as in many higher order theories, the approximation $\sigma_z = 0$ is retained in the present model. The strain–displacement relations and the electric field–potential relations for the directions x, z are

$$\varepsilon_x = u_{,x}, \quad \varepsilon_z = w_{,z}, \quad \gamma_{zx} = u_{,z} + w_{,x}; \quad E_x = -\phi_{,x}, \quad E_z = -\phi_{,z}, \tag{1}$$

where a subscript comma denotes differentiation. Unlike most other studies, E_x is not considered as zero, since it is an electric field induced by the piezoelectric coupling. With these assumptions,

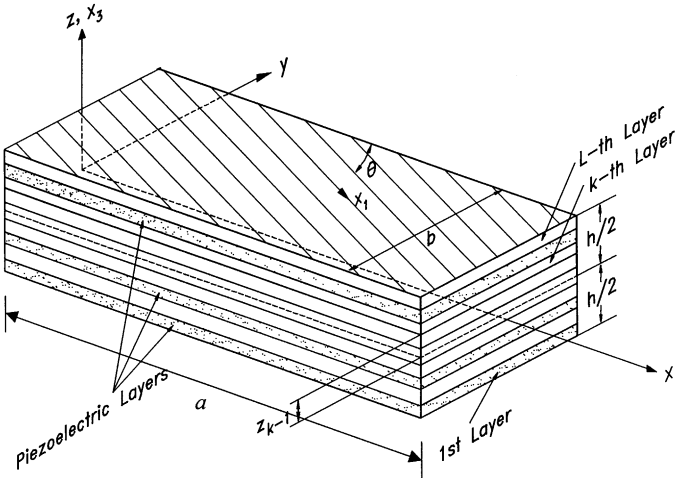

Fig. 1. Geometry of hybrid beam.

the general 3-D constitutive equations for stresses and electric displacements D_x, D_z reduce to [19]

$$\begin{bmatrix} \sigma_x \\ D_z \end{bmatrix} = \begin{bmatrix} \hat{Q}_{11} & -\hat{e}_{31} \\ \hat{e}_{31} & \hat{\eta}_{33} \end{bmatrix} \begin{bmatrix} \varepsilon_x \\ E_z \end{bmatrix}, \quad \begin{bmatrix} \tau_{zx} \\ D_x \end{bmatrix} = \begin{bmatrix} \hat{Q}_{55} & -\hat{e}_{15} \\ \hat{e}_{15} & \hat{\eta}_{11} \end{bmatrix} \begin{bmatrix} \gamma_{zx} \\ E_x \end{bmatrix}, \tag{2}$$

where $\hat{Q}_{11}, \hat{Q}_{55}, \hat{e}_{31}, \hat{e}_{15}, \hat{\eta}_{11}, \hat{\eta}_{33}$ are related to Young's moduli Y_i, shear moduli G_{ij}, the Poisson ratios v_{ij}, piezoelectric strain constants d_{ij}, dielectric constants ε_{ij} and the orientation of the material symmetry axes with respect to the x-axis.

The potential field is assumed as piecewise linear between n_ϕ points z_ϕ^j, $j = 1, 2, \ldots, n_\phi$, across the thickness h [21] with $z_\phi^1 = z_0, z_\phi^{n_\phi} = z_L$ and

$$\phi(x, z, t) = \Psi_\phi^j(z)\phi^j(x, t), \tag{3}$$

where $\phi^j(x, t) = \phi(x, z_\phi^j, t)$. $\Psi_\phi^j(z)$ are linear interpolation functions. The summation convention is used for the repeated index j and for j' used later. n_ϕ can differ from L and is determined by the accuracy required of ϕ. This enables piecewise linear modelling of ϕ in the piezoelectric layers by dividing them into sublayers. Two-dimensional exact piezoelasticity solutions [3,19] have revealed that for moderately thick hybrid beams under electric potential load, the deflection w has significant variation across the thickness of the piezoelectric layers. This is due to the significant contribution to ε_z by the electric field through the d_{33} coefficient. However, σ_x has negligible contribution to ε_z. Hence to introduce this effect in the present 1-D model, the deflection w is not approximated as uniform across the thickness. Instead the deflection w is approximated by integrating the constitutive equation for ε_z by neglecting the contribution of σ_x: $\varepsilon_z = w_{,z} = -v_{xz}\sigma_x/Y_x + d_{33}E_z \simeq -d_{33}\phi_{,z}$. Then

$$w(x, z, t) = w_0(x, t) - \bar{\Psi}_\phi^j(z)\phi^j(x, t), \tag{4}$$

where $\bar{\Psi}_\phi^j(z) = \int_0^z d_{33}\Psi_{\phi,z}^j(z)\,\mathrm{d}z$ is a piecewise linear function.

The axial displacement u for the kth layer is assumed [21,24] as a combination of a third order global variation across the thickness h with layerwise linear variation:

$$u(x, z, t) = u_k(x, t) - zw_{0,x}(x, t) + z\psi_k(x, t) + z^2\xi(x, t) + z^3\eta(x, t), \tag{5}$$

where u_k and ψ_k denote the translation and rotation variables of the kth layer. In all third order zigzag theories [24], the term $(-zw_{0,x})$ in Eq. (5) is required to satisfy the shear traction-free conditions at the top and the bottom and the shear continuity conditions at the layer interfaces. Eqs. (2)–(5) yield

$$\tau_{zx} = \hat{Q}_{55}^k(\psi_k + 2z\xi + 3z^2\eta) + [\hat{e}_{15}^k\Psi_\phi^j(z) - \hat{Q}_{55}^k\bar{\Psi}_\phi^j(z)]\phi_{,x}^j. \tag{6}$$

For the k_0th layer denote $u(x, 0, t) = u_0(x, t) = u_{k_0}(x, t)$, $\psi_{k_0}(x, t) = \psi_0(x, t)$. The functions u_k, ψ_k, ξ, η are expressed, as in Ref. [21], in terms of u_0, w_0, ψ_0, ϕ^j, using the $(L-1)$ conditions each for the continuity of τ_{zx} and u at the layer interfaces and the two shear traction-free conditions $\tau_{zx} = 0$ at $z = z_0, z_L$. Thus

$$u(x, z, t) = u_0(x, t) - zw_{0,x}(x, t) + R^k(z)\psi_0(x, t) + R^{kj}(z)\phi_{,x}^j(x, t), \tag{7}$$

where the cubic functions $R^k(z), R^{kj}(z)$ are listed in Eq. (A.1) in Appendix A. Thus ϕ, w, u are expressed by Eqs. (3), (4), and (7) in terms of the primary variables u_0, w_0, ψ_0 and ϕ^j. The number of the primary displacement variables is three which is the same as in the FSDT.

The dynamic field equations and the variationally consistent boundary conditions are formulated using extended Hamilton's principle for a piezoelectric continuum [25]:

$$\int_{t_1}^{t_2}\left[\int_V(\rho\dot{u}_i\delta\dot{u}_i-\sigma_{ij}\delta\varepsilon_{ij}-D_i\delta\phi_{,i})\,\mathrm{d}V+\int_\Gamma(T_i^{\,n}\delta u_i+D_n\delta\phi)\,\mathrm{d}\Gamma - \sum_{i=1}^{\bar{n}_\phi}\int_{A^{j_i}}(D_{z_u}-D_{z_l})\delta\phi^{j_i}\,\mathrm{d}A^{j_i}\right]\mathrm{d}t=0 \tag{8}$$

with $(\delta u_i, \delta\phi, \delta\phi^{j_i})=0$ at times $t=t_1,t_2$. The overdot represents differentiation with respect to time. V and Γ are the volume and surface area of the beam and ρ is the mass density. A^{j_i} is an internal surface $z=z_\phi^{j_i}$ where ϕ^{j_i} is prescribed and $D_{z_l}-D_{z_u}=q_{j_i}$ is the extraneous surface charge density on this surface. The subscripts u and l in D_{z_u} and D_{z_l} refer to the faces of the interface at $(z_\phi^{j_i})^+,(z_\phi^{j_i})^-$. The total number of such prescribed potentials is $\bar{n}_\phi$. D_n is the surface charge density and $T_i^{\,n}$ are the stress vector components. Let p_z^1, p_z^2 be the forces per unit area applied on the bottom and top surfaces of the beam in direction z. Let there be distributed viscous resistance force with the distributed viscous damping coefficient c_1 per unit area per unit transverse velocity of the top surface of the beam.

The field equations are formulated in terms of beam inertia elements $I_{kl}, I_{k4}^j, I_{44}^{jj'}, \bar{I}_{22}, \bar{I}_{24}^j, \bar{I}_{44}^{jj'}$, beam stress resultants N_x, M_x, P_x, Q_x, S_x^j, $\bar{Q}_x^j$, beam electric displacement resultants H^j, G^j, beam damping coefficients $\hat{c}_1, c_\phi^j, c_\phi^{jj'}$ and the beam mechanical and electrical loads F_2, F_4^j, which are defined in Eqs. (A.2)–(A.6) in Appendix A. The coupled field equations of dynamics consist of the following three equations of motion and n_ϕ equations for the electric potentials:

$$\begin{aligned}
&I_{11}\ddot{u}_0-I_{12}\ddot{w}_{0,x}+I_{13}\ddot{\psi}_0+I_{14}^{j'}\ddot{\phi}_{,x}^{j'}-N_{x,x}=0,\\
&\quad -I_{12}\ddot{u}_{0,x}+I_{22}\ddot{w}_{0,xx}-\bar{I}_{22}\ddot{w}_0-I_{23}\ddot{\psi}_{0,x}-I_{24}^{j'}\ddot{\phi}_{,xx}^{j'}+\bar{I}_{24}^{j'}\ddot{\phi}^{j'}+M_{x,xx}-\hat{c}_1\dot{w}_0+c_\phi^{j'}\dot{\phi}^{j'}+F_2=0,\\
&I_{13}\ddot{u}_0-I_{23}\ddot{w}_{0,x}+I_{33}\ddot{\psi}_0+I_{34}^{j'}\ddot{\phi}_{,x}^{j'}-P_{x,x}+Q_x=0,\\
&I_{14}^{j}\ddot{u}_{0,x}-I_{24}^{j}\ddot{w}_{0,xx}+\bar{I}_{24}^{j}\ddot{w}_0+I_{34}^{j}\ddot{\psi}_{0,x}+I_{44}^{jj'}\ddot{\phi}_{,xx}^{j'}-\bar{I}_{44}^{jj'}\ddot{\phi}^{j'}\\
&\quad -S_{x,xx}^j+\bar{Q}_{x,x}^j+H_{,x}^j-G^j+c_\phi^j\dot{w}_0-c_\phi^{jj'}\dot{\phi}^{j'}+F_4^j=0,\quad j=1,2,\ldots,n_\phi.
\end{aligned} \tag{9}$$

The essential or natural boundary conditions at the ends at $x=0,a$ are

$$\begin{aligned}
&u_0=u_0^*\quad\text{or}\quad N_x=N_x^*,\\
&w_0=w_0^*\quad\text{or}\quad -I_{21}\ddot{u}_0+I_{22}\ddot{w}_{0,x}-I_{23}\ddot{\psi}_0-I_{24}^{j'}\ddot{\phi}_{,x}^{j'}+M_{x,x}=\langle\tau_{zx}\rangle^*,\\
&w_{0,x}=w_{0,x}^*\quad\text{or}\quad M_x=M_x^*,\\
&\psi_0=\psi_0^*,\quad\text{or}\quad P_x=P_x^*,
\end{aligned}$$

$$\phi^j = \phi^{j*} \quad \text{or} \quad I_{41}^j \ddot{u}_0 - I_{42}^j \ddot{w}_{0,x} + I_{43}^j \ddot{\psi}_0 + I_{44}^{jj'} \ddot{\phi}_{,x}^{j'} + H^j - S_{x,x}^j + \bar{Q}_x^j = H^{j*} - \langle \Psi_\phi^j(z)\tau_{zx} \rangle^*,$$
$$\phi_{,x}^j = \phi_{,x}^{j*} \quad \text{or} \quad S_x^j = S_x^{j*}, \tag{10}$$

where * denotes a prescribed value.

The coupled electro-mechanical dynamic equations in terms of the primary variables u_0, w_0, ψ_0, ϕ^j are obtained by substitution of the expressions of the resultants of stresses and electric displacements from Eq. (A.4) into Eq. (9)

$$\bar{L}\ddot{\bar{U}} + \hat{L}\dot{\bar{U}} + L\bar{U} = \bar{P}, \tag{11}$$

where

$$\bar{U} = [\,u_0 \quad w_0 \quad \psi_0 \quad \phi^1 \quad \phi^2 \quad \ldots \quad \phi^{n_\phi}\,]^{\mathrm{T}}, \quad \bar{P} = [\,P_1 \quad P_2 \quad P_3 \quad P_4^1 \quad P_4^2 \quad \ldots \quad P_4^{n_\phi}\,]^{\mathrm{T}}. \tag{12}$$

$\bar{L}$ and L are symmetric matrices of linear differential operators in x and $\hat{L}$ is a symmetric matrix. Their elements are listed in Eqs. (A.7) and (A.8) in Appendix A. After solving for $\bar{U}$, τ_{zx} is obtained by integrating the 2-D equation of motion in the x direction to yield $\tau_{zx} = \int_{-h/2}^{z} (\rho\ddot{u} - \sigma_{x,x})\,\mathrm{d}z$.

3. An assessment of zigzag theory for beams

In order to assess the accuracy of the coupled zigzag theory developed herein, analytical solution is obtained for simply-supported beams with the following boundary conditions at $x = 0, a$:

$$N_x = 0, \quad w_0 = 0, \quad M_x = 0, \quad P_x = 0, \quad \phi^j = 0, \quad S_x^j = 0, \quad j = 1, \ldots, n_\phi \tag{13}$$

and compared with the exact piezoelastic solution [2,3]. The solution of Eq. (11) is expanded in Fourier series as

$$(w_0, \phi^j, N_x, M_x, P_x, S_x^j, G^j, p_z^i, q_j) = \sum_{n=1}^{\infty} (w_0, \phi^j, N_x, M_x, P_x, S_x^j, G^j, p_z^i, q_j)_n \sin \bar{n}x,$$
$$(u_0, \psi_0, Q_x, \bar{Q}_x^j, H^j) = \sum_{n=1}^{\infty} (u_0, \psi_0, Q_x, \bar{Q}_x^j, H^j)_n \cos \bar{n}x \tag{14}$$

with $\bar{n} = n\pi/a$. Substituting these in Eq. (11) yields for an nth Fourier component, the coupled equations

$$M\ddot{\bar{U}}^n + C\dot{\bar{U}}^n + K\bar{U}^n = \bar{P}^n, \tag{15}$$

where $\bar{U}^n, \bar{P}^n$ are the nth Fourier components of $\bar{U}, \bar{P}$. The elements of the symmetric inertia, damping and stiffness matrices M, C, K are not listed for brevity.

$\bar{U}$ is partitioned into a set of three mechanical displacement variables U, a set of unknown output voltages Φ_s at z_ϕ^j's where ϕ is not prescribed and a set of known input actuation voltages Φ_a at the active actuated surfaces. $\bar{P}$ is partitioned into a set of three mechanical loads P, a set of known input electric loads Q_s at z_ϕ^j's where ϕ is not prescribed and a set of unknown output electrical loads Q_a at the actuated interfaces. Eq. (15) can be partitioned and re-arranged so that

these can be solved for a beam in active/sensory/active–sensory mode for steady state response under harmonic electromechanical load and for natural frequencies of free oscillations.

For free undamped vibration at natural frequency ω_n, Eq. (15) reduces to an eigenvalue problem. Consider response under longitudinally sinusoidal [i.e., varying as $\sin(n\pi x/a)$] electromechanical harmonic load at forcing frequency ω:

$$P^n = P_0^n \cos \omega t, \quad \Phi_a^n = \Phi_{a_0}^n \cos \omega t, \quad Q_s^n = Q_{s_0}^n \cos \omega t. \tag{16}$$

Let the steady state damped response be

$$\tilde{U}^n = [\, U^n \quad \Phi_s^n \,]^{\mathrm{T}} = \tilde{U}_0^n \cos \omega t + \tilde{U}_0^{n*} \sin \omega t, \quad Q_a^n = Q_{a_0}^n \cos \omega t + Q_{a_0}^{n*} \sin \omega t. \tag{17}$$

Substituting from Eqs. (16) and (17) into Eq. (15) and equating separately the $\cos \omega t$ and the $\sin \omega t$ terms to zero, yields algebraic equations for $\tilde{U}_0^n, \tilde{U}_0^{n*}, Q_{a_0}^n, Q_{a_0}^{n*}$.

Results are presented for three highly inhomogeneous simply-supported hybrid beams (a), (b) and (c) (Fig. 2). All these beams consist of an elastic substrate with a piezoelectric layer of PZT-5A [26] of thickness $0.1h$ bonded to its top. The PZT-5A layers have poling in $+z$ direction. The top and the bottom of the substrate are grounded. The stacking order is mentioned from the bottom. Beam (a) has a 5-ply substrate of thickness $0.09h/0.225h/0.135h/0.18h/0.27h$ of materials 1/2/3/1/3 which have highly inhomogeneous stiffness in tension and shear and is a good test case [27]. The substrate of beam (b) is a graphite-epoxy composite (material 4 [26]) laminate with 4 layers of equal thickness $0.225h$ with lay-up $[0^\circ/90^\circ/90^\circ/0^\circ]$. The substrate of beam (c) is a three-layer sandwich with graphite-epoxy faces and a soft core [23] with thicknesses $0.09h/0.72h/0.09h$. The top surface of PZT layer is subjected to either closed circuit condition (C) for which the surface potential ϕ^{n_ϕ} is prescribed or open circuit condition (O) for which the applied surface charge density at the top $q_{n_\phi} = 0$. Convergence studies have revealed that converged results are obtained by discretizing the electric field across the PZT layer by piecewise linear variation across four equal sublayers. The material properties are: $[(Y_1, Y_2, Y_3, G_{12}, G_{23}, G_{31}), \nu_{12}, \nu_{13}, \nu_{23}] =$

Material 1: [(6.9, 6.9, 6.9, 1.38, 1.38, 1.38) GPa, 0.25, 0.25, 0.25]
Material 2: [(224.25, 6.9, 6.9, 56.58, 1.38, 56.58) GPa, 0.25, 0.25, 0.25]
Material 3: [(172.5, 6.9, 6.9, 3.45, 1.38, 3.45) GPa, 0.25, 0.25, 0.25]
Material 4: [(181, 10.3, 10.3, 7.17, 2.87, 7.17) GPa, 0.28, 0.28, 0.33]
Face: [(131.1, 6.9, 6.9, 3.588, 2.3322, 3.588) GPa, 0.32, 0.32, 0.49]

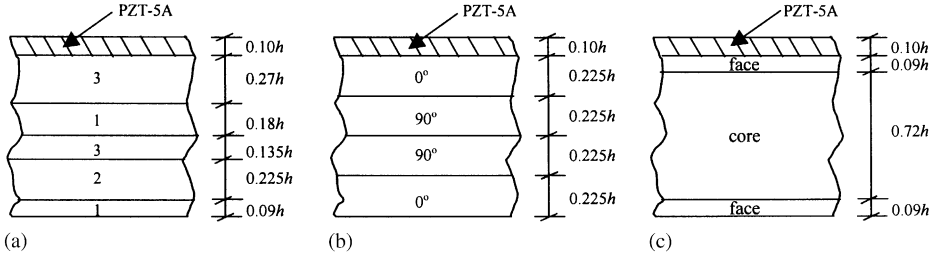

Fig. 2. Configurations of beams (a)–(c).

Core: $[(0.2208, 0.2001, 2760, 16.56, 455.4, 545.1)\ \text{MPa}, 0.99, 3\times10^{-5}, 3\times10^{-5}]$
PZT-5A: $[(61.0, 61.0, 53.2, 22.6, 21.1, 21.1)\ \text{GPa}, 0.35, 0.38, 0.38]$,

and $[(d_{31}, d_{32}, d_{33}, d_{15}, d_{24}), (\eta_{11}, \eta_{22}, \eta_{33})] = [(-171, -171, 374, 584, 584)\times10^{-12}\ \text{m/V}, (1.53, 1.53, 1.5)\times10^{-8}\ \text{F/m}]$. The density of materials 1, 2, 3, 4 is 1578 kg/m^3 and of PZT-5A, face, and core is 7600, 1000 and 70 kg/m^3, respectively.

The accuracy of the present theory is assessed by comparison with the exact 2-D piezoelasticity solution [3]. Since the number of displacement variables in the present theory is the same as in the FSDT, results are also compared with the FSDT. The shear correction factor for the FSDT solution is taken as $\frac{5}{6}$. No comparison is done with other layerwise theories which involve more displacement unknowns, since the accuracy of the present theory is established directly by comparison with the exact solution.

Table 1
Exact natural frequencies $\bar{\omega}_n$ (open circuit condition) and % error of zigzag theory (Pres.) and FSDT

n	Mode	S	Test beam (a)			Composite beam (b)			Sandwich beam (c)		
			Exact	Pres.	FSDT	Exact	Pres.	FSDT	Exact	Pres.	FSDT
1	1	5	5.8909	0.45	48.56	5.5344	0.55	16.82	3.9675	0.99	61.19
		10	8.1605	0.32	18.48	7.4425	0.25	6.66	6.2158	0.48	27.24
		20	9.4811	0.13	5.00	8.3699	0.08	1.64	7.8633	0.18	8.17
		100	10.087	0.00	−0.34	8.7552	−0.01	−0.42	8.7586	0.04	−0.33
	2	5	9.6540	3.76	15.20	7.4406	3.12	2.28	5.7993	1.39	4.73
		10	10.844	0.67	5.34	7.8294	0.86	0.64	6.2114	0.43	4.81
		20	11.356	0.13	1.26	7.9667	0.23	−0.02	6.5865	0.14	1.66
		100	11.539	0.00	−0.14	8.0159	0.01	−0.26	6.8108	0.01	−0.66
	3	5	3.0370	3.92	48.64	2.3379	7.16	18.92	2.6665	1.47	22.47
		10	1.9759	1.44	101.3	1.7711	1.42	23.48	1.6109	0.12	52.92
		20	1.6264	0.86	136.0	1.5685	0.61	28.69	1.2040	0.09	84.97
		100	1.5049	0.71	152.0	1.4966	0.41	31.13	1.0458	0.20	105.33
2	1	5	15.140	2.61	78.11	13.625	1.34	24.59	8.9317	2.53	86.79
		10	23.563	0.45	48.57	22.137	0.56	16.82	15.870	0.99	61.19
		20	32.642	0.33	18.48	29.770	0.25	6.66	24.863	0.48	27.24
		100	40.014	0.03	0.37	34.811	0.02	−0.13	34.528	0.03	0.80
3	1	5	25.673	10.53	83.85	22.058	3.66	24.25	14.254	5.59	88.61
		10	41.171	0.95	68.41	38.128	0.83	22.48	25.669	1.61	79.19
		20	62.007	0.41	34.24	57.829	0.42	12.18	44.033	0.74	46.21
		100	88.836	0.05	1.51	77.576	0.03	0.31	75.850	0.07	2.67
5	1	5	44.742	46.58	95.84	41.458	8.63	14.99	25.907	16.71	80.31
		10	81.317	5.75	82.09	71.214	2.24	24.84	46.167	3.84	89.02
		20	128.53	0.59	60.00	120.29	0.68	20.21	82.998	1.27	71.91
		100	237.03	0.13	5.00	209.25	0.08	1.64	196.58	0.18	8.17

The frequencies and the modal entities are non-dimensionalized as follows with $S = a/h$:

$$\bar{\omega} = \omega_n a S_1(\rho_0/Y_0)^{1/2}, \quad (\bar{u}, \bar{w}, \bar{\phi}) = (u, w, 10^3\phi S d_0)/\max(u, w),$$
$$(\bar{\sigma}_x, \bar{\tau}_{zx}) = (\sigma_x, \tau_{zx})Sh/Y_0 \max(u, w),$$

where $\max(u, w)$ denotes the largest value of u and w through the thickness for a particular mode and $S_1 = S, 1, 1/S$ for the first three thickness modes, respectively. $Y_0 = 6.9$ GPa for beams (a) and (c) and $Y_0 = 10.3$ GPa for beam (b), $d_0 = 374 \times 10^{-12}\,\mathrm{CN}^{-1}$, $\rho_0 = 1000\ \mathrm{kg/m^3}$ for beam (c) and $\rho_0 = 1578\ \mathrm{kg/m^3}$ for the other beams.

The dimensionless natural frequencies obtained by the exact 2-D piezoelasticity solution, and the percentage error of the zigzag theory (Zigzag) and the uncoupled FSDT solutions, are given in Table 1 for beams (a)–(c) with open circuit condition. The frequencies are listed for the bending, shear, and extension modes 1, 2, 3 for $n = 1$ and for only the flexural mode 1 for $n = 2, 3, 5$. Similar results for the closed circuit condition are presented in Table 2. The maximum error in the present zigzag theory is 5.8% for the first five bending modes of moderately thick beams with $S = 10$% and 10.6% for the first three bending modes of thick beams with $S = 5$. By contrast, the corresponding errors in the FSDT are 89.0% and 88.6% with large errors for the sandwich beam (c). For a thin beam with $S = 20$, the maximum error in the zigzag theory is only 1.3% for the first five bending modes whereas it is 71.9% for the FSDT. The error in the FSDT for thin beams with $S = 20$ for the second bending mode itself is not small, being 18.5%, 6.7% and 27.2% for beams (a), (b), (c), respectively. The error in the FSDT in most cases is atleast one order more than the

Table 2
Exact bending natural frequencies $\bar{\omega}_n$ (closed circuit condition) and % error of zigzag theory (Pres.)

n	S	Beam (a)		Beam (b)		Beam (c)	
		Exact	Pres.	Exact	Pres.	Exact	Pres.
1	5	5.8727	0.49	5.5165	0.58	3.9537	1.00
	10	8.1253	0.34	7.4119	0.26	6.1856	0.48
	20	9.4318	0.14	8.3308	0.08	7.8128	0.18
	100	10.028	0.02	8.7134	−0.02	8.6959	0.01
2	5	15.108	2.64	13.589	1.36	8.9001	2.52
	10	23.491	0.48	22.066	0.58	15.815	1.00
	20	32.501	0.34	29.647	0.26	24.742	0.48
	100	39.788	0.03	34.643	0.01	34.277	0.03
3	5	25.628	10.57	22.002	3.68	14.197	5.54
	10	41.069	0.99	38.020	0.86	25.583	1.62
	20	61.784	0.44	57.620	0.44	43.860	0.75
	100	88.345	0.06	77.204	0.03	75.318	0.07
5	5	44.676	46.71	39.307	14.38	25.809	16.57
	10	81.164	5.78	71.027	2.27	45.992	3.82
	20	128.18	0.63	119.93	0.71	82.720	1.28
	100	235.80	0.14	208.27	0.08	195.32	0.18

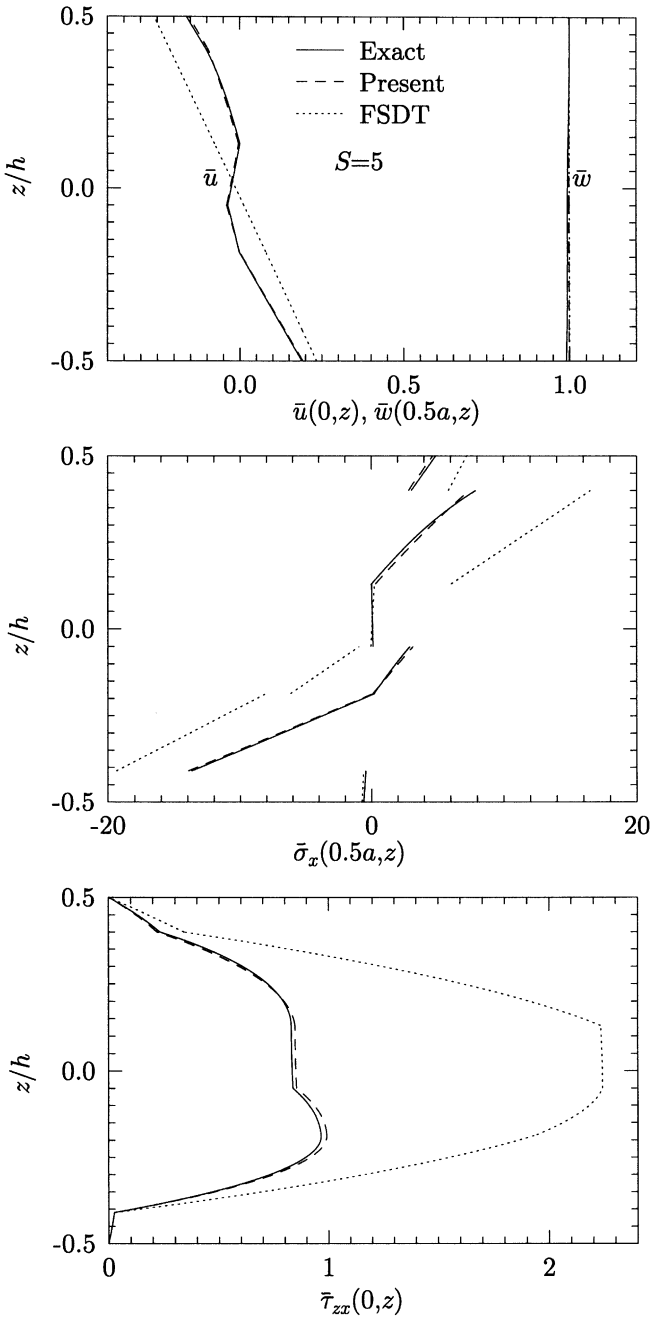

Fig. 3. Distributions of $\bar{u}$, $\bar{w}$, $\bar{\sigma}_x$, $\bar{\tau}_{zx}$ in the fundamental thickness mode of a thick ($S = 5$) test beam (a).

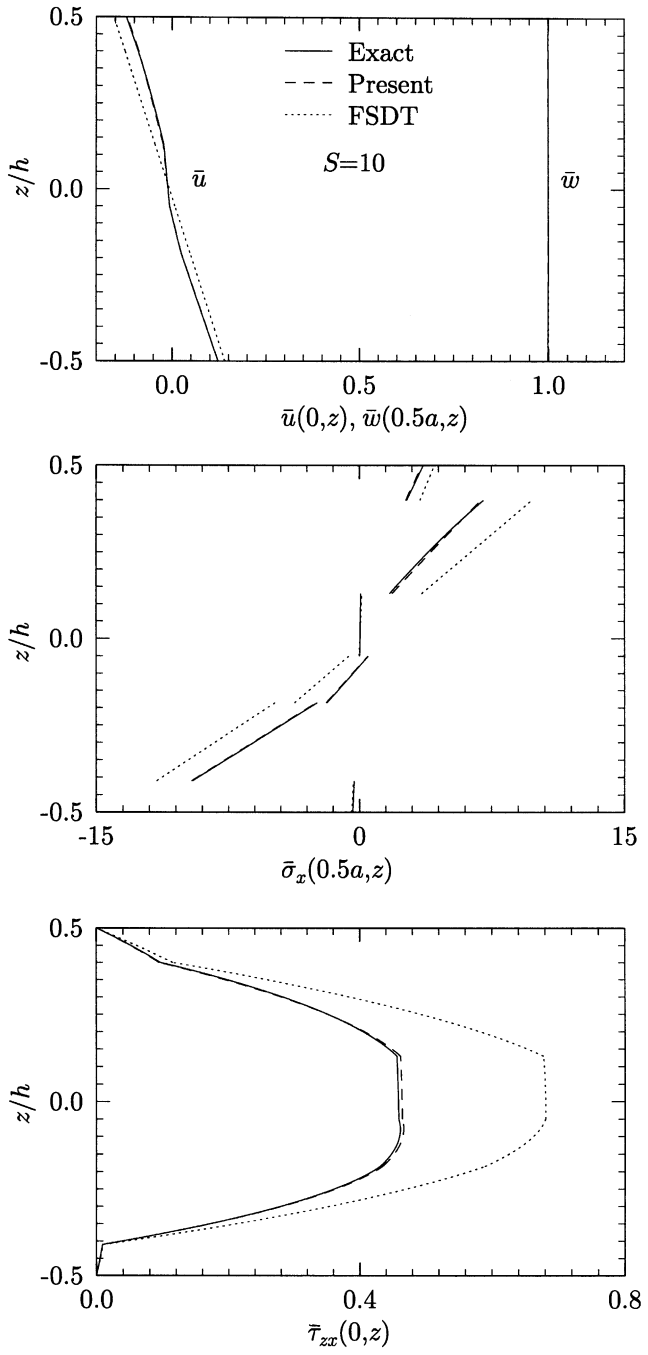

Fig. 4. Distributions of $\bar{u}$, $\bar{w}$, $\bar{\sigma}_x$, $\bar{\tau}_{zx}$ in the fundamental thickness mode of a moderately thick ($S = 10$) test beam (a).

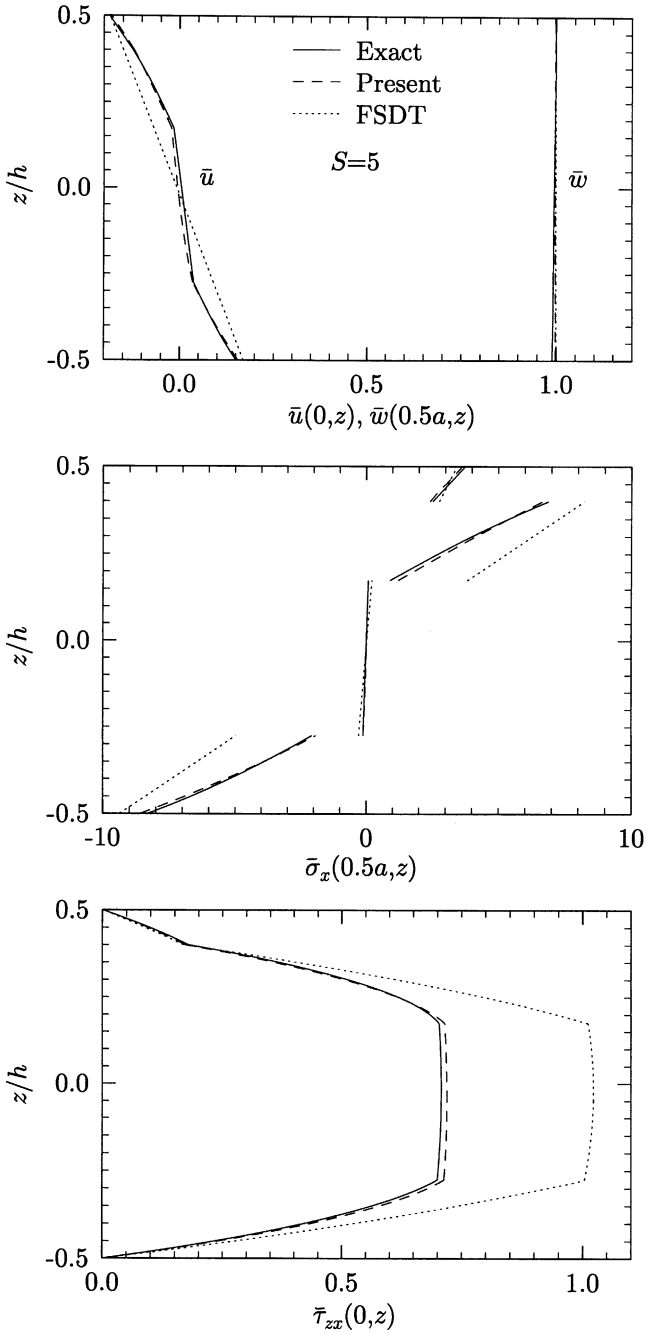

Fig. 5. Distributions of $\bar{u}$, $\bar{w}$, $\bar{\sigma}_x$, $\bar{\tau}_{zx}$ in the fundamental thickness mode of a thick ($S = 5$) composite beam (b).

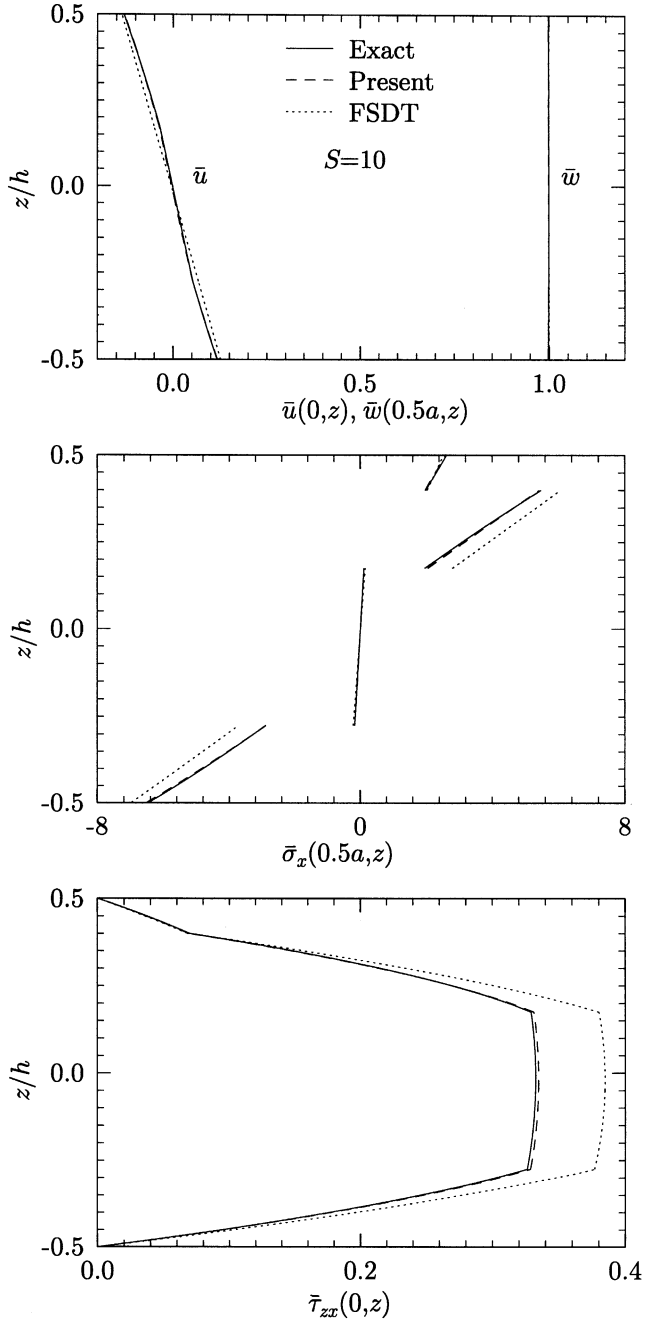

Fig. 6. Distributions of $\bar{u}$, $\bar{w}$, $\bar{\sigma}_x$, $\bar{\tau}_{zx}$ in the fundamental thickness mode of a moderately thick ($S = 10$) composite beam (b).

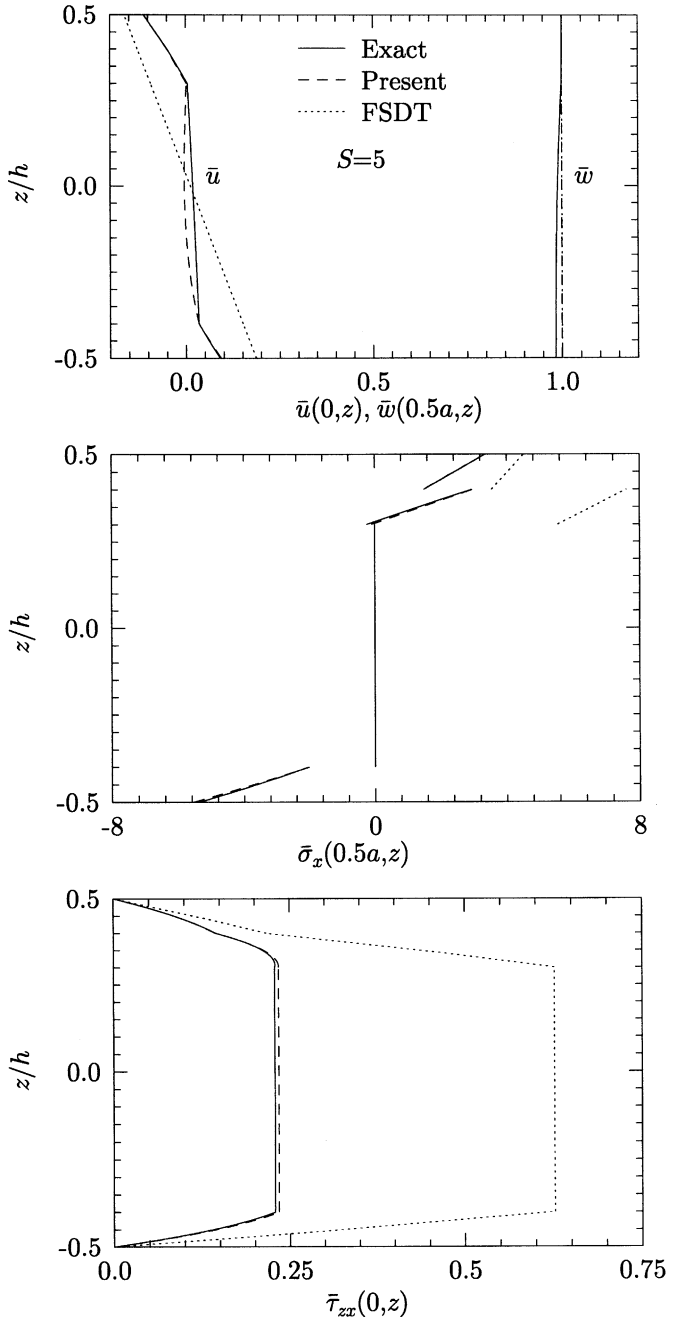

Fig. 7. Distributions of $\bar{u}$, $\bar{w}$, $\bar{\sigma}_x$, $\bar{\tau}_{zx}$ in the fundamental thickness mode of a thick ($S = 5$) sandwich beam (c).

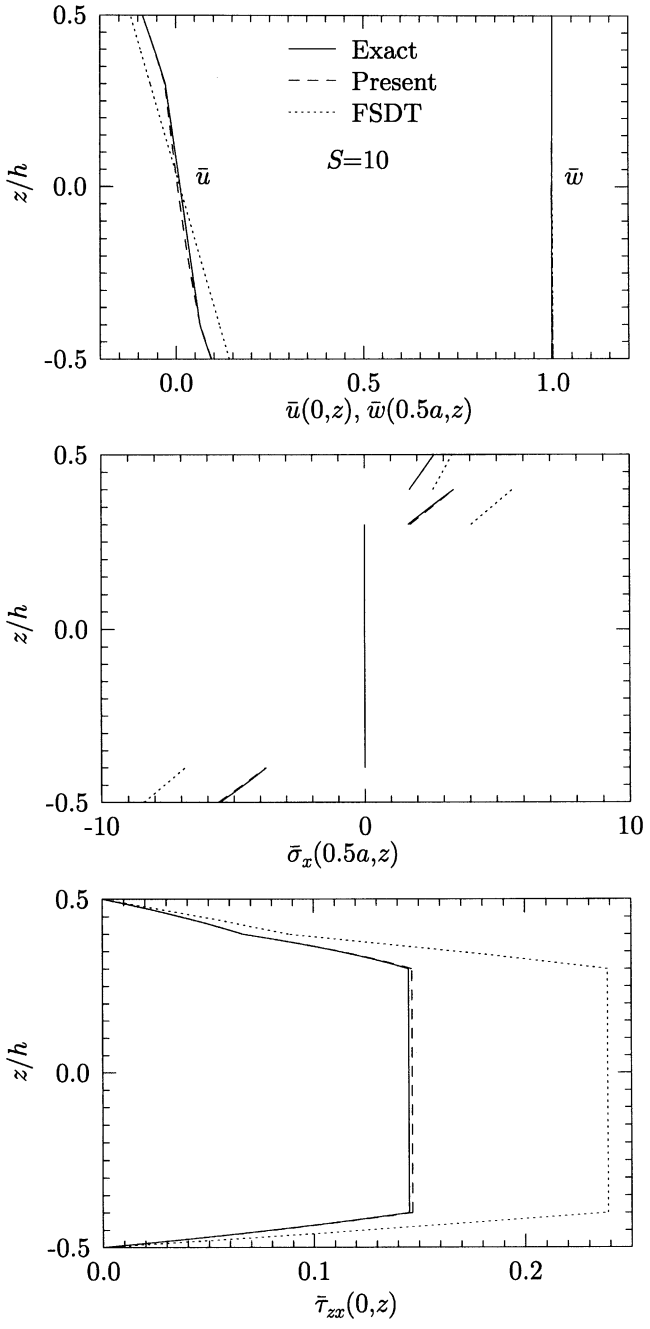

Fig. 8. Distributions of $\bar{u}$, $\bar{w}$, $\bar{\sigma}_x$, $\bar{\tau}_{zx}$ in the fundamental thickness mode of a moderately thick ($S = 10$) sandwich beam (c).

error in the zigzag theory. The present zigzag theory has been able to predict quite accurately the effect of the open and closed circuit conditions on ω_n.

The through-the-thickness distributions of modal displacements $\bar{u}$, $\bar{w}$ and stresses $\bar{\sigma}_x$, $\bar{\tau}_{zx}$ in the fundamental thickness mode (flexural) are shown in Figs. 3–8 for thick and moderately thick beams (a)–(c) at open circuit condition for $n = 1$. The present results for $\bar{u}$, $\bar{w}$ $\bar{\sigma}_x$, $\bar{\tau}_{zx}$, including the slope discontinuities in $\bar{u}$ at the layer interfaces, are in excellent agreement with the exact 2-D solution for both thick and thin hybrid beams with all kinds of substrate: a test case, symmetric composite and sandwich. By contrast, the errors in the FSDT for $\bar{u}$, $\bar{\sigma}_x$, $\bar{\tau}_{zx}$, are quite large, with the errors increasing for the thicker beams wherein the simplified kinematic assumptions do not hold well. The errors in the FSDT mode shapes are especially large for the test beam (a) and the sandwich beam (c).

Consider steady state forced response of beams for two load cases:

1. Harmonic pressure excitation $p_z^2 = p_0 \sin \bar{n}x \cos \omega t$ on the top surface with open circuit condition $q_{n_\phi} = 0$ on it.

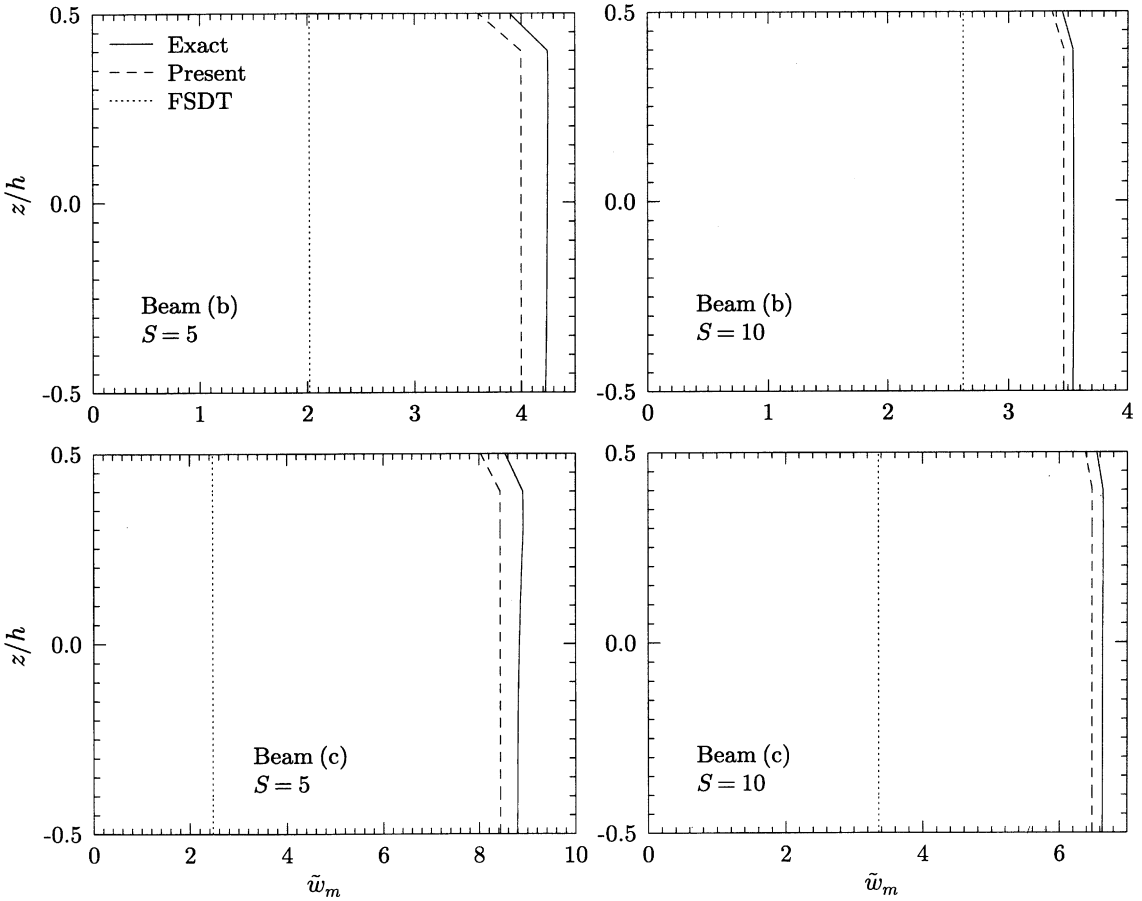

Fig. 9. Distributions of amplitude $\tilde{w}_m(0.5a, z)$ for load case 2 ($\omega/\omega_1 = 0.8, n = 1, \bar{c} = 0$).

2. Applied harmonic actuation potential on the top surface $\phi(x, h/2, t) = \phi^{n_\phi} = \phi_0 \sin \bar{n}x \cos \omega t$ (closed circuit condition).

Let the deflection of the centre of the beam be $w(a/2, 0, t) = w_m \cos(\omega t - \kappa)$ with amplitude w_m and phase lag κ. The following non-dimensional variables are used for w_m, ϕ_0, forcing frequency ω and damping constant c_1:

$$\tilde{w}_m = 100 w_m Y_0/hS^4 p_0, \quad \tilde{\phi}_0 = 10^4 \phi_0 Y_0 d_0/hS^2 p_0 \text{ (case 1)}; \quad \tilde{w}_m = 10 w_m/S^2 d_0 \phi_0 \text{ (case 2)},$$

$$\bar{\omega} = \omega Sa(\rho_0/Y_0)^{1/2}, \quad \bar{c} = c_1 S/2\rho_0 a\omega_n.$$

The through-the-thickness distributions of the amplitude of deflection $\tilde{w}_m(0.5a, z)$ for beams (b) and (c) for potential load case 2 are compared in Fig. 9 for $n = 1, \omega/\omega_1 = 0.8, \bar{c} = 0$ and $S = 5, 10$. The present zigzag model is able to predict the non-uniform distribution of deflection amplitude across the thickness quite accurately. The FSDT is unable to predict non-uniform profile of the deflection across the thickness and yields very inaccurate results.

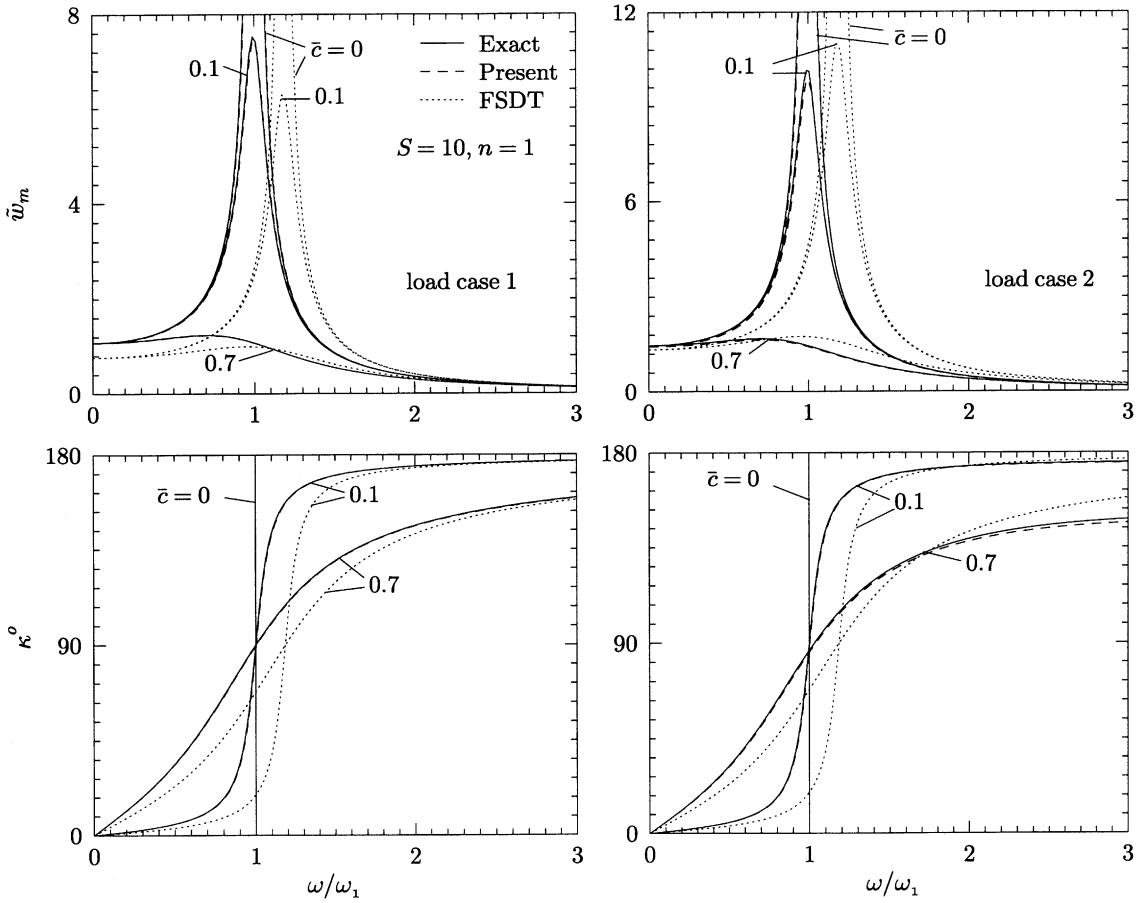

Fig. 10. Amplitude $\tilde{w}_m$ and phase κ for test beam (a) under the load cases 1 and 2.

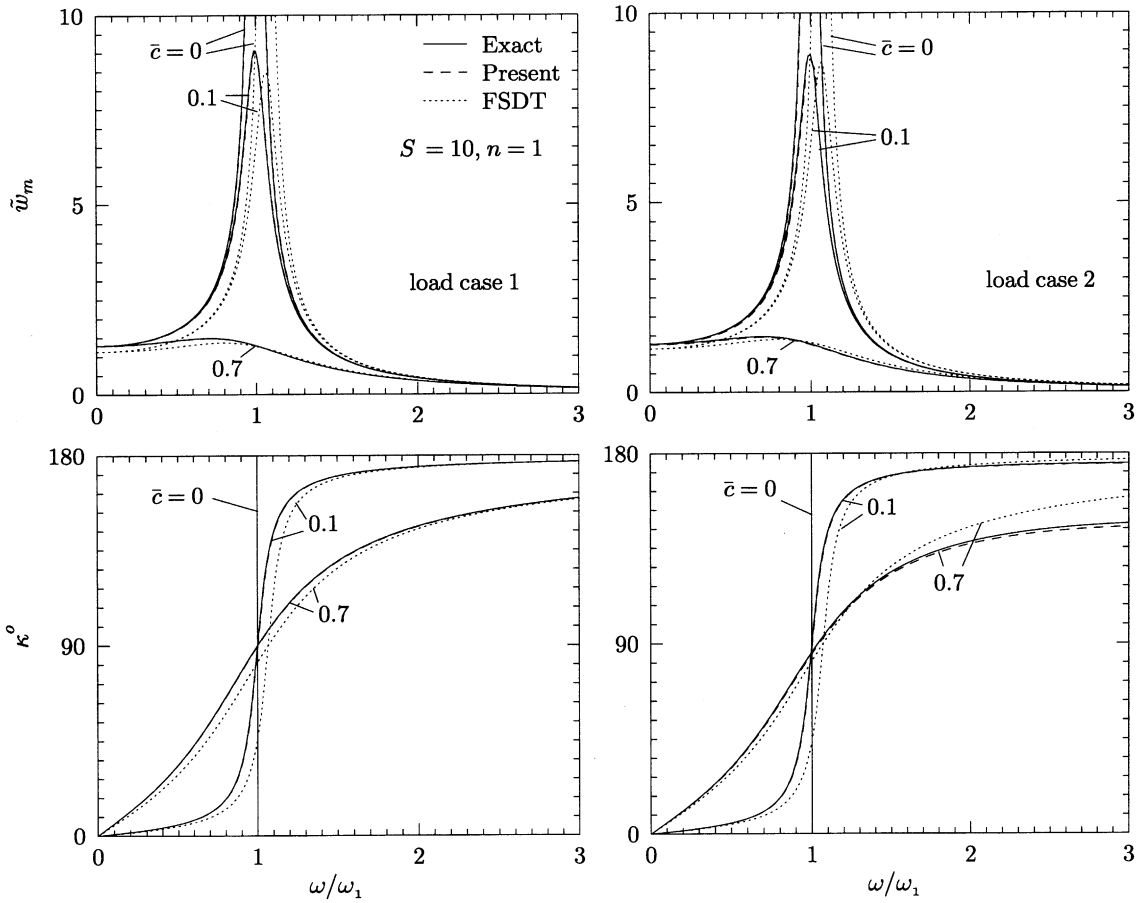

Fig. 11. Amplitude $\tilde{w}_m$ and phase κ for composite beam (b) under the load cases 1 and 2.

The amplitude $\tilde{w}_m$ and phase lag κ of the central deflection for the two load cases are presented for $S = 10$ in Figs. 10, 11 and 12 as a function of the forcing frequency, for longitudinal spatial mode $n = 1$ for beams (a), (b), and (c), respectively. Undamped ($\bar{c} = 0$), lightly damped ($\bar{c} = 0.1$) and heavily damped ($\bar{c} = 0.7$) cases are considered. The percentage errors of the amplitude $\tilde{w}_m$ and the phase κ in the zigzag theory and the FSDT are compared in Figs. 13 and 14 for the two loadings for the lightly damped case of $\bar{c} = 0.1$ for thick ($S = 5$), moderately thick ($S = 10$) and thin ($S = 20$) beams. It is observed from Figs. 10–14 that the present zigzag theory predicts the amplitude and phase of the forced harmonic response very accurately for all beams for both load cases and the three damping cases for the whole frequency range except for small errors for thick ($S = 5$) beams in the neighbourhood of the natural frequency ω_1. In contrast, the error in the FSDT for both amplitude and phase is quite large in the whole range of frequency for moderately thick and thick beams with the error increasing in the neighbourhood of ω_1. In the range $\omega > \omega_1$, the error in the deflection amplitude for the FSDT is much larger for the potential load case 2

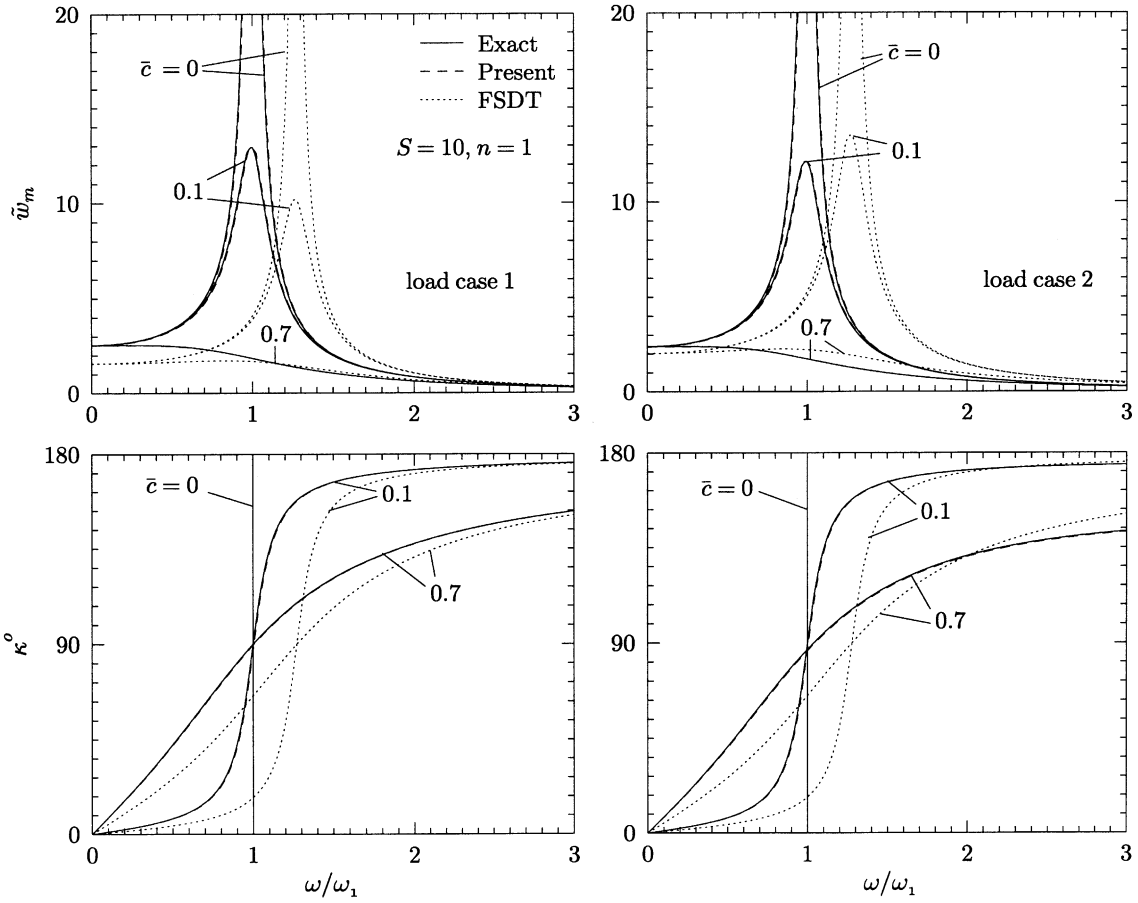

Fig. 12. Amplitude $\tilde{w}_m$ and phase κ for sandwich beam (c) under the load cases 1 and 2.

compared to the mechanical load case 1. Even for the lightly damped thin beams with $S = 20, \bar{c} = 0.1$, the maximum errors in the FSDT are quite large being 18.2%, 6.4%, 22.4% for w_m and 23.4%, 8.4%, 28.0% for κ for load case 1 and 28.9%, 8.6%, 37.7% for w_m and 25.3%, 10.4%, 29.7% for κ for load case 2 for the beams (a), (b), (c), respectively. One source of error in $\tilde{w}_m$ in the FSDT is due to the error of the induced transverse strain due to piezoelectricity from the d_{33} coefficient. Similar trend was observed in the statics case using the layerwise theory [19] for beam and the coupled FSDT for rectangular plate [28]. The error in $\tilde{w}_m$ in the FSDT is large since it is the cumulative effect of the errors in predicting the static deflection, the natural frequency and the dynamic magnification factor for the forced response. The deflection amplitude and phase response curves of test beam (a) for the third longitudinal mode $n = 3$ are compared in Fig. 15 for $S = 10$. The zigzag theory yields quite accurate results for this higher mode also, with small error in the phase for all ω/ω_3 and small error in $\tilde{w}_m$ in the neighbourhood of $\omega/\omega_3 = 1$. The errors in the FSDT for this higher mode $n = 3$ are much larger than those for the fundamental mode $n = 1$.

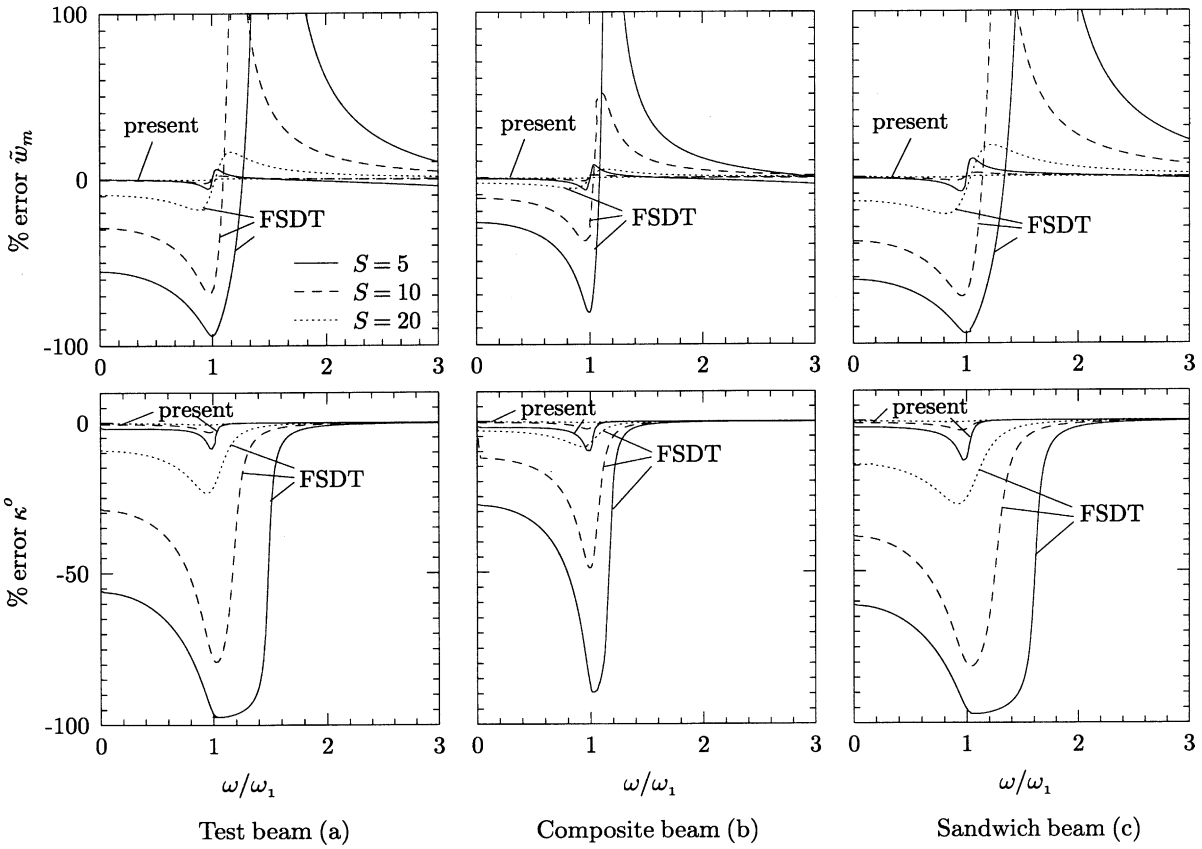

Fig. 13. Percentage error of present theory and FSDT for amplitude $\tilde{w}_m$ and phase κ under load case 1 for $n=1,\ \bar{c}=0.1$.

The amplitude $\bar{w}_m$ and phase κ of the composite beam (b) with $S=10, \bar{c}=0.1$, under harmonic pressure and actuation potential, are presented in Fig. 16. It is observed that the zigzag solution agrees very well with the exact 2-D solution but the FSDT solution has large error. It is concluded from Fig. 16 that the application of a passive actuation potential has almost the same percentage reduction of deflection amplitude for the whole range of ω/ω_1.

4. Conclusions

The new coupled zigzag theory presented for the dynamic analysis of hybrid composite and sandwich beams with any lay-up, is the *first dynamic theory of hybrid beams* in which the *conditions on the transverse shear stress*, at the top, bottom, and layer interfaces *are satisfied exactly*, even for the case of non-zero longitudinal electric field. The effect of the piezoelectric transverse normal strain is accounted for in the transverse displacement field. The theory has the

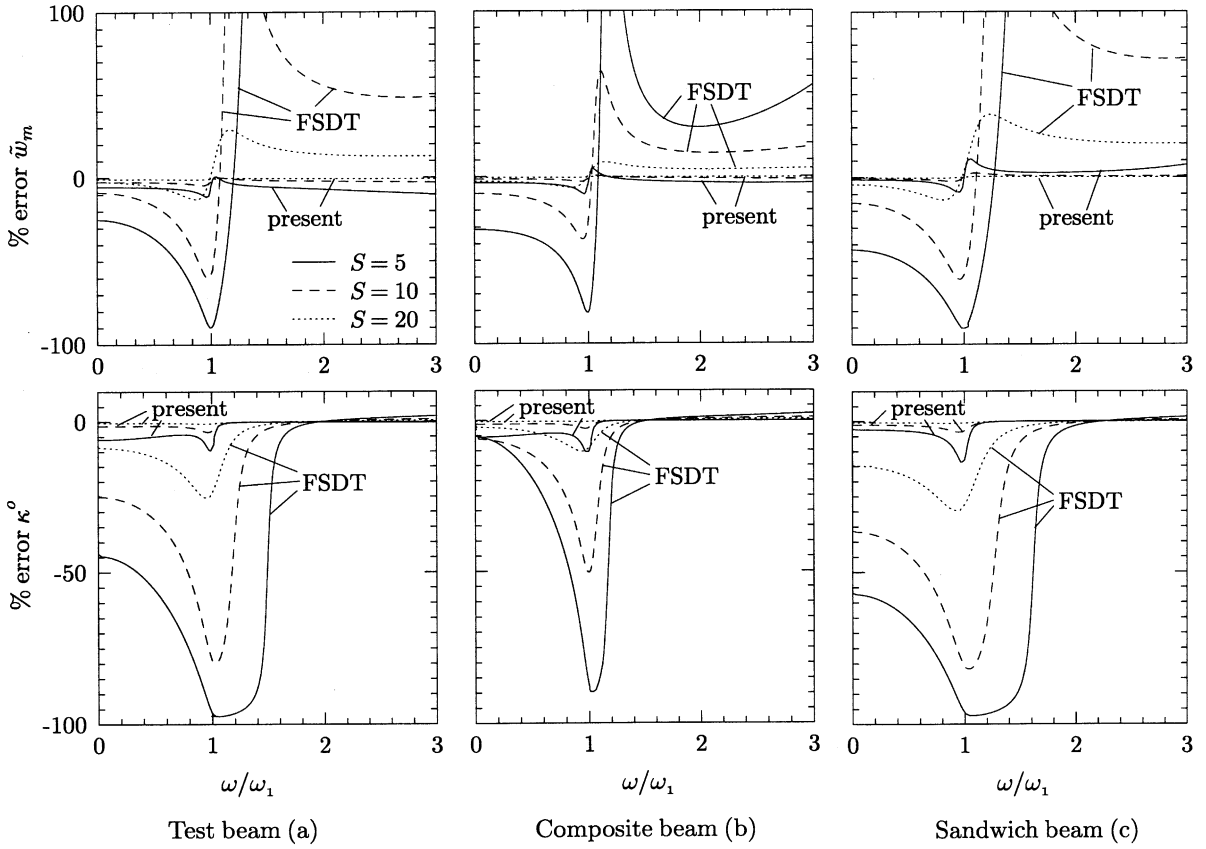

Fig. 14. Percentage error of present theory and FSDT for amplitude $\tilde{w}_m$ and phase κ under load case 2 for $n = 1$, $\bar{c} = 0.1$.

capability to model accurately the variation of potential across sensor and actuator layers by appropriate piecewise linear approximation. The present theory can effectively model closed circuit as well as open circuit electric boundary conditions in the piezoelectric layer as required in sensory and active applications. The accuracy of this theory is established by comparison with the exact 2-D piezoelasticity solutions for beams of highly heterogeneous lay-ups with elastic substrate consisting of a test case, a symmetric composite one and a sandwich one. The zigzag theory yields very accurate values of natural frequencies, modal displacements and stresses, and steady state undamped and damped forced response under harmonic electromechanical loads in the whole frequency range for moderately thick and thin highly heterogeneous beams and a small error for the thick beams. Unlike other layerwise theories, the present accurate theory is also economical since the number of primary displacement variables is the same as that of the FSDT. The error in the FSDT is large for natural frequencies of higher modes and for moderately thick beams. The error of the FSDT solution for forced response is large for moderately thick and even thin beams with $S = 10$, especially for the test beam and the sandwich beam.

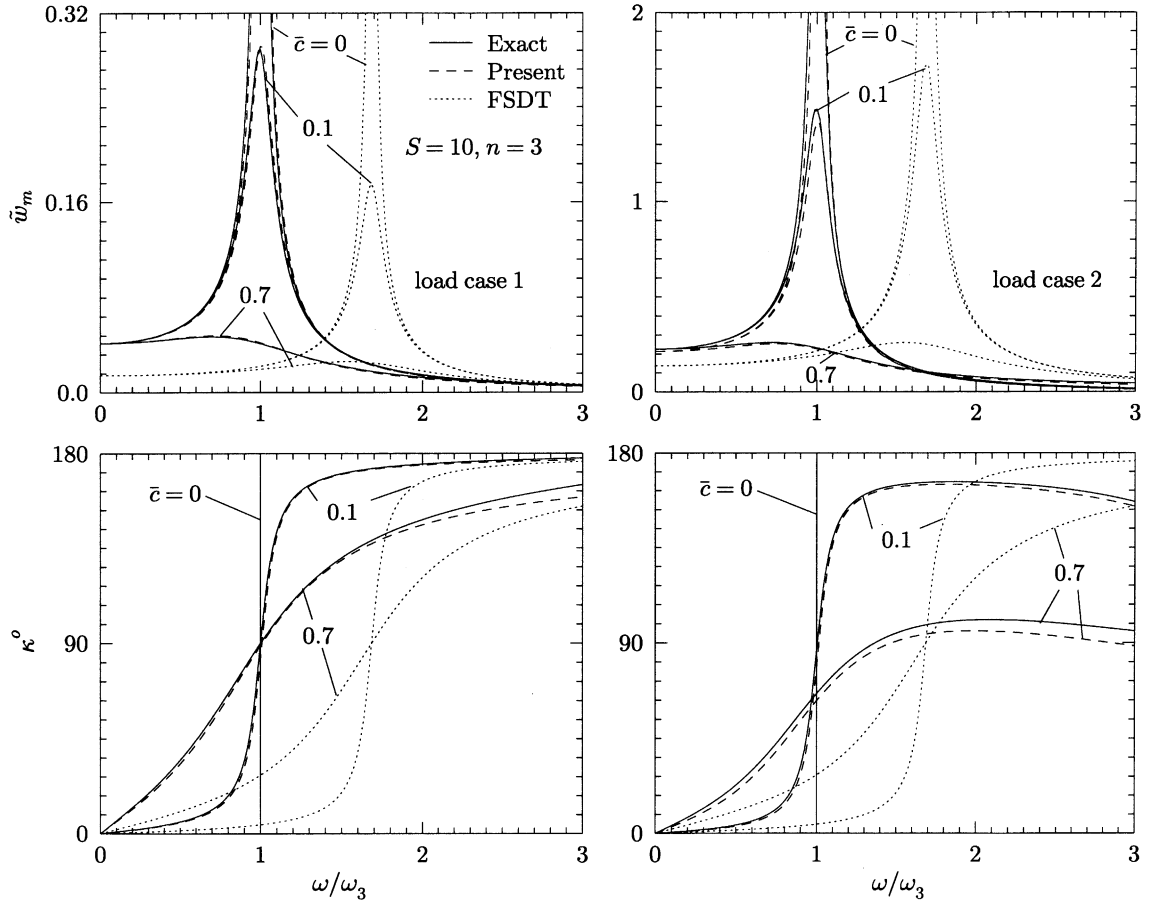

Fig. 15. Amplitude $\tilde{w}_m$ and phase κ for test beam (a) under load cases 1 and 2 ($n = 3$).

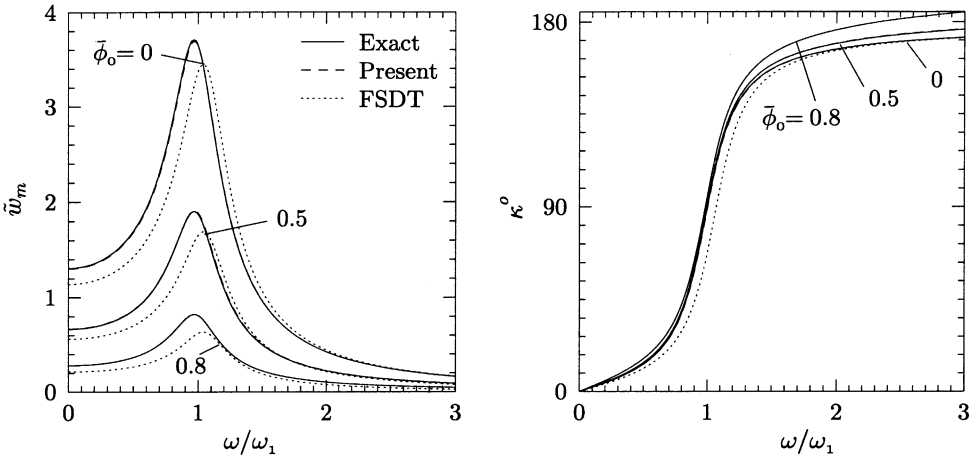

Fig. 16. Amplitude $\tilde{w}_m$ and phase κ for composite beam (b) under harmonic pressure with actuation potential.

Acknowledgements

The authors thank the reviewers for their constructive comments which have led to improvement of the paper. This work has been financially supported by a research grant from SERC, DST, Government of India.

Appendix A

The expressions for the functions $R^k(z), R^{kj}(z)$ are given by

$$R^k(z) = R_k(z)/R_2^{k_0} = \hat{R}_1^k + z\hat{R}_2^k + z^2\hat{R}_3 + z^3\hat{R}_4,$$

$$R^{kj}(z) = R_{k\phi}^j(z) - R_k(z)R_{j1}^{k_0}/R_2^{k_0} = \hat{R}_1^{kj} + z\hat{R}_{j1}^k + z^2\hat{R}_5^j + z^3\hat{R}_6^j$$

with

$$(\hat{R}_1^k, \hat{R}_2^k, \hat{R}_3, \hat{R}_4) = (R_1^k, R_2^k, R_3, R_4)/R_2^{k_0},$$

$$\begin{aligned}
&\hat{R}_1^{kj} = R_1^{kj} - \hat{R}_1^k R_{j1}^{k_0}, \quad \hat{R}_5^j = R_5^j - \hat{R}_3 R_{j1}^{k_0},\\
&\hat{R}_{j1}^k = R_{j1}^k - \hat{R}_2^k R_{j1}^{k_0}, \quad \hat{R}_6^j = R_6^j - \hat{R}_4 R_{j1}^{k_0},\\
&R_1^k = \bar{R}_2^k - \bar{R}_2^{k_0}, \quad R_k(z) = R_1^k + zR_2^k + z^2R_3 + z^3R_4,\\
&R_1^{kj} = \bar{R}_{j1}^k - \bar{R}_{j1}^{k_0}, \quad R_{k\phi}^j(z) = R_1^{kj} + zR_{j1}^k + z^2R_5^j + z^3R_6^j,\\
&\bar{R}_2^k = \sum_{i=2}^{k} z_{i-1}(R_2^{i-1} - R_2^i), \quad \bar{R}_{j1}^k = \sum_{i=2}^{k} z_{i-1}(R_{j1}^{i-1} - R_{j1}^i),\\
&R_2^k = a_1^k R_3 + a_2^k R_4, \quad R_{j1}^k = a_1^k R_5^j + a_2^k R_6^j + [C_{3j}^k - \hat{e}_{15}^k \Psi_\phi^j(z_k)]/\hat{Q}_{55}^k + \bar{\Psi}_\phi^j(z_k),\\
&a_1^k = 2(C_1^k/\hat{Q}_{55}^k - z_k), \quad a_2^k = 3(2C_2^k/\hat{Q}_{55}^k - z_k^2),\\
&R_3 = 4C_2^L/\Delta, \quad R_5^j = -(2z_0^2C_{3j}^L + 4C_2^L C_5^j)/\Delta, \quad \Delta = 4z_0^2C_1^L - 8z_0C_2^L,\\
&R_4 = -4C_1^L/3\Delta, \quad R_6^j = (4z_0C_{3j}^L + 4C_1^L C_5^j)/3\Delta,\\
&C_1^k = \sum_{i=1}^{k} \hat{Q}_{55}^i(z_i - z_{i-1}), \quad C_{3j}^k = \sum_{i=1}^{k} [\hat{e}_{15}^i\{\Psi_\phi^j(z_i) - \Psi_\phi^j(z_{i-1})\} - \hat{Q}_{55}^i\{\bar{\Psi}_\phi^j(z_i) - \bar{\Psi}_\phi^j(z_{i-1})\}],\\
&C_2^k = \sum_{i=1}^{k} \hat{Q}_{55}^i(z_i^2 - z_{i-1}^2)/2, \quad C_5^j = \bar{\Psi}_\phi^j(z_0) - \hat{e}_{15}^1\Psi_\phi^j(z_0)/\hat{Q}_{55}^1.
\end{aligned} \tag{A.1}$$

The beam damping coefficients are defined by

$$\hat{c}_1 = bc_1, \quad c_\phi^j = bc_1\bar{\Psi}_\phi^j(z_L), \quad c_\phi^{jj'} = bc_1\bar{\Psi}_\phi^j(z_L)\bar{\Psi}_\phi^{j'}(z_L). \tag{A.2}$$

Using the notation $\langle \cdots \rangle = \sum_{k=1}^{L} \int_{z_{k-1}^{+}}^{z_k^{-}} (\ldots) b \, \mathrm{d}z$, the beam inertia elements are defined by

$$
\begin{aligned}
&[I_{11}, I_{12}, I_{13}, I_{14}^{j'}] = \langle \rho[1, z, R^k(z), R^{kj'}(z)] \rangle, \quad I_{44}^{jj'} = \langle \rho R^{kj}(z) R^{kj'}(z) \rangle, \\
&[I_{22}, I_{23}, I_{24}^{j'}] = \langle \rho z[z, R^k(z), R^{kj'}(z)] \rangle, \quad [\bar{I}_{22}, \bar{I}_{24}^{j'}] = \langle \rho[1, \Psi_\phi^{j'}(z)] \rangle, \\
&[I_{33}, I_{34}^{j'}] = \langle \rho R^k(z)[R^k(z), R^{kj'}(z)] \rangle, \quad \bar{I}_{44}^{jj'} = \langle \rho \Psi_\phi^{j}(z) \Psi_\phi^{j'}(z) \rangle.
\end{aligned} \tag{A.3}
$$

The beam stress resultants $N_x, M_x, P_x, Q_x, S_x^j, \bar{Q}_x^j$ and the beam electric displacement resultants H^j, G^j are defined by

$$
\begin{aligned}
N_x &= \langle \sigma_x \rangle = A_{11} u_{0,x} - A_{12} w_{0,xx} + A_{13} \psi_{0,x} + A_{14}^{j'} \phi_{,xx}^{j'} + \beta_1^{j'} \phi^{j'}, \\
M_x &= \langle z \sigma_x \rangle = A_{12} u_{0,x} - A_{22} w_{0,xx} + A_{23} \psi_{0,x} + A_{24}^{j'} \phi_{,xx}^{j'} + \beta_2^{j'} \phi^{j'}, \\
P_x &= \langle R^k(z) \sigma_x \rangle = A_{13} u_{0,x} - A_{23} w_{0,xx} + A_{33} \psi_{0,x} + A_{34}^{j'} \phi_{,xx}^{j'} + \beta_3^{j'} \phi^{j'}, \\
S_x^j &= \langle R^{kj}(z) \sigma_x \rangle = A_{14}^{j} u_{0,x} - A_{24}^{j} w_{0,xx} + A_{34}^{j} \psi_{0,x} + A_{44}^{jj'} \phi_{,xx}^{j'} + \beta_4^{jj'} \phi^{j'}, \\
Q_x &= \langle R_{,z}^k(z) \tau_{zx} \rangle = \bar{A}_{33} \psi_0 + (\bar{A}_{34}^{j'} + \bar{\beta}_3^{j'}) \phi_{,x}^{j'}, \\
\bar{Q}_x^j &= \langle [R_{,z}^{kj}(z) - \bar{\Psi}_\phi^j(z)] \tau_{zx} \rangle = \bar{A}_{34}^{j} \psi_0 + (\bar{A}_{44}^{jj'} + \bar{\beta}_4^{jj'}) \phi_{,x}^{j'}, \\
H^j &= \langle \Psi_\phi^j(z) D_x \rangle = \bar{\beta}_3^{j} \psi_0 + (\bar{\beta}_4^{j'j} - \bar{E}^{jj'}) \phi_{,x}^{j'}, \\
G^j &= \langle \Psi_{\phi,z}^j(z) D_z \rangle = \beta_1^j u_{0,x} - \beta_2^j w_{0,xx} + \beta_3^j \psi_{0,x} + \beta_4^{j'j} \phi_{,xx}^{j'} - E^{jj'} \phi^{j'}.
\end{aligned} \tag{A.4}
$$

The elements of the beam stiffness $A, \bar{A}$; the beam electro-mechanical coupling matrices $\beta^{j'}, \bar{\beta}^{j'}$ and the beam dielectric matrices $E^{jj'}, \bar{E}^{jj'}$ are defined in terms of the material constants by

$$
\begin{aligned}
&[A_{11}, A_{12}, A_{13}, A_{14}^{j'}, A_{22}, A_{23}, A_{24}^{j'}, A_{33}] = \langle \hat{Q}_{11}[1, z, R^k(z), R^{kj'}(z), z^2, zR^k(z), zR^{kj'}(z), \{R^k(z)\}^2] \rangle, \\
&[A_{34}^{j'}, A_{44}^{jj'}] = \langle \hat{Q}_{11}[R^k(z) R^{kj'}(z), R^{kj}(z) R^{kj'}(z)] \rangle, \\
&[\bar{A}_{33}, \bar{A}_{34}^{j'}, \bar{A}_{44}^{jj'}] = \langle \hat{Q}_{55}[\{R_{,z}^k(z)\}^2, R_{,z}^k(z)\{R_{,z}^{kj'}(z) - \bar{\Psi}_\phi^{j'}(z)\}, \{R_{,z}^{kj}(z) - \bar{\Psi}_\phi^{j}(z)\}\{R_{,z}^{kj'}(z) - \bar{\Psi}_\phi^{j'}(z)\}] \rangle, \\
&[\beta_1^{j'}, \beta_2^{j'}, \beta_3^{j'}, \beta_4^{jj'}] = \langle \hat{e}_{31} \Psi_{\phi,z}^{j'}(z)[1, z, R^k(z), R^{kj}(z)] \rangle, \\
&[\bar{\beta}_3^{j'}, \bar{\beta}_4^{jj'}] = \langle \hat{e}_{15} \Psi_\phi^{j'}(z)[R_{,z}^k(z), R_{,z}^{kj}(z) - \bar{\Psi}_\phi^{j}(z)] \rangle, \\
&E^{jj'} = \langle \hat{\eta}_{33} \Psi_{\phi,z}^{j}(z) \Psi_{\phi,z}^{j'}(z) \rangle, \quad \bar{E}^{jj'} = \langle \hat{\eta}_{11} \Psi_\phi^{j}(z) \Psi_\phi^{j'}(z) \rangle.
\end{aligned} \tag{A.5}
$$

The mechanical load F_2 and electrical loads F_4^j are defined by

$$
F_2 = b(p_z^1 + p_z^2), \quad F_4^j = b[-p_z^1 \bar{\Psi}_\phi^j(z_0) - p_z^2 \bar{\Psi}_\phi^j(z_L) + D_z(x, z_L, t) \delta_{jn_\phi} - D_z(x, z_0, t) \delta_{j1} + q_{j_i} \delta_{jj_i}], \tag{A.6}
$$

where δ_{ij} is Kronecker's delta.

The elements of the operators $\bar{L}$ and L are given by

$$\begin{aligned}
&\bar{L}_{11} = I_{11}, \quad \bar{L}_{12} = -I_{12}()_{,x},\\
&\bar{L}_{13} = I_{13}, \quad \bar{L}_{1,3+j'} = I_{14}^{j'}()_{,x},\\
&\bar{L}_{22} = I_{22}()_{,xx} - \bar{I}_{22}, \quad \bar{L}_{23} = -I_{23}()_{,x},\\
&\bar{L}_{2,3+j'} = -I_{24}^{j'}()_{,xx} + \bar{I}_{24}^{j'}, \quad \bar{L}_{33} = I_{33},\\
&\bar{L}_{3,3+j'} = I_{34}^{j'}()_{,x}, \quad \bar{L}_{3+j,3+j'} = I_{44}^{jj'}()_{,xx} - \bar{I}_{44}^{jj'},\\
&L_{11} = -A_{11}()_{,xx}, \quad L_{12} = A_{12}()_{,xxx},\\
&L_{13} = -A_{13}()_{,xx}, \quad L_{1,3+j'} = -A_{14}^{j'}()_{,xxx} - \beta_1^{j'}()_{,x},\\
&L_{22} = -A_{22}()_{,xxxx}, \quad L_{23} = A_{23}()_{,xxx},\\
&L_{2,3+j'} = A_{24}^{j'}()_{,xxxx} + \beta_2^{j'}()_{,xx}, \quad L_{33} = -A_{33}()_{,xx} + \bar{A}_{33},\\
&L_{3,3+j'} = -A_{34}^{j'}()_{,xxx} + [-\beta_3^{j'} + \bar{A}_{34}^{j'} + \bar{\beta}_3^{j'}]()_{,x}, \quad P_1 = P_3 = 0, \quad P_2 = -F_2,\\
&L_{3+j,3+j'} = -A_{44}^{j}()_{,xxxx} + [-\beta_4^{jj'} - \beta_4^{j'j} + \bar{A}_{44}^{jj'} - \bar{E}^{jj'} + \bar{\beta}_4^{jj'} + \bar{\beta}_4^{j'j}]()_{,xx} + E^{jj'}, \quad P_4^{j} = -F_4^{j},
\end{aligned} \tag{A.7}$$

for $(j,j') = 1, \ldots, n_\phi$. The non-zero elements of $\hat{L}$ are

$$\hat{L}_{22} = -\hat{c}_1, \quad \hat{L}_{2,3+j'} = \hat{L}_{3+j',2} = c_\phi^{j'}, \quad \hat{L}_{3+j,3+j'} = -c_\phi^{jj'}. \tag{A.8}$$

Appendix B. Nomenclature

$A_{kl}, A_{k4}^{j}, A_{44}^{jj'}, \bar{A}_{33}, \bar{A}_{34}^{j}, \bar{A}_{44}^{jj'}$	elements of beam stiffness matrices
a, b, h	length, width, and thickness of the beam
$d_{ij}, e_{ij}; \varepsilon_{ij}, \eta_{ij}$	piezoelectric strain and stress constants; dielectric constants, permittivities
$E_x, E_y, E_z; D_x, D_z; \phi$	electric field components, electric displacements, electric potential
$E^{jj'}, \hat{E}^{jj'}$	elements of beam dielectric matrices
G^{j}, H^{j}	electric displacement resultants
$G_{zx}, Y_x; \rho$	shear and Young's moduli; density
$I_{kl}, I_{k4}^{j}, I_{44}^{jj'}, \bar{I}_{22}, \bar{I}_{24}^{j}, \bar{I}_{44}^{jj'}$	beam inertia elements
M, C, K	inertia, damping and stiffness matrices
$N_x, M_x, P_x, Q_x, S_x^{j}, \bar{Q}_x^{j}$	stress resultants
S	thickness parameter a/h
$\bar{U}, \bar{P}$	displacement and electric potential vector, load vector
$u, w; u_0, w_0, \psi_0$	displacements, mid-plane displacements and shear rotation
x, y, z	co-ordinates in axial, width and thickness directions
$\sigma_x, \tau_{zx}; \varepsilon_x, \varepsilon_z, \gamma_{xz}$	stresses; strains
$\Psi_\phi^{j}(z)$	interpolation functions

ω_n, ω natural and forcing frequencies
$\beta_k^j, \beta_4^{jj'}, \bar{\beta}_3^j, \bar{\beta}_4^{jj'}$ elements of beam electromechanical coupling matrices

References

[1] D.A. Saravanos, P.R. Heyliger, Mechanics and computational models for laminated piezoelectric beams, plates and shells, *Applied Mechanics Review* 52 (1999) 305–320.

[2] P.R. Heyliger, S.B. Brooks, Exact free vibration of piezoelectric laminates in cylindrical bending, *International Journal of Solids and Structures* 32 (1995) 2945–2960.

[3] S. Kapuria, P.C. Dumir, A. Ahmed, Exact 2D piezoelasticity solution of hybrid beam with damping under harmonic electromechanical load, *Journal of Applied Mathematics and Mechanics (ZAMM)*, in press.

[4] S.K. Ha, C. Keilers, F.K. Chang, Three-dimensional finite element analysis of composite structures containing distributed piezoceramic sensors and actuators, *American Institute of Aeronautics and Astronautics Journal* 30 (1992) 772–780.

[5] T. Bailey, J.E. Hubbard, Distributed piezoelectric–polymer active vibration control of a cantilever beam, *Journal of Guidance, Control and Dynamics* 8 (1985) 605–611.

[6] S. Im, S.N. Atluri, Effects of a piezo-actuator on a finitely deformed beam subject to general loading, *American Institute of Aeronautics and Astronautics Journal* 27 (1989) 1801–1807.

[7] R. Chandra, I. Chopra, Structural modelling of composite beams with induced-strain actuators, *American Institute of Aeronautics and Astronautics Journal* 31 (1993) 1692–1701.

[8] D.H. Robbins, J.N. Reddy, Analysis of piezoelectrically actuated beams using a layer-wise displacement theory, *Computers and Structures* 41 (1991) 265–279.

[9] H.S. Tzou, Distributed sensing and controls of flexible plates and shells using distributed piezoelectric element, *Journal of Wave Material Interaction* 4 (1989) 11–29.

[10] X.D. Zhang, C.T. Sun, Formulation of an adaptive sandwich beam, *Smart Materials and Structures* 5 (1996) 814–823.

[11] K. Chandrashekhara, P. Donthireddy, Vibration suppression of composite beams with piezoelectric devices using a higher order theory, *European Journal of Mechanics A/Solids* 16 (1997) 709–721.

[12] X.Q. Peng, K.Y. Lam, G.R. Liu, Active vibration control of composite beams with piezoelectrics: a finite element model with third order theory, *Journal of Sound and Vibration* 209 (1998) 635–650.

[13] A. Benjeddou, M.A. Trindadade, R. Ohayon, A unified beam finite element model for extension and shear piezoelectric actuation mechanisms, *Journal of Intelligent Materials Systems and Structures* 8 (1997) 1012–1025.

[14] S.S. Vel, R.C. Batra, Analysis of piezoelectric bimorphs and plates with segmented actuators, *Thin-walled Structures* 39 (2001) 23–44.

[15] D. Huang, B. Sun, Approximate analytical solutions of smart composite Mindlin beams, *Journal of Sound and Vibration* 244 (2001) 379–394.

[16] J.A. Mitchell, J.N. Reddy, A refined hybrid plate theory for composite laminates with piezoelectric laminae, *International Journal of Solids and Structures* 32 (1995) 2345–2367.

[17] X. Zhou, A. Chattopadhyay, H. Gu, Dynamic responses of smart composite using a coupled thermo-piezoelectric-mechanical model, *American Institute of Aeronautics and Astronautics Journal* 38 (2000) 1939–1948.

[18] D.A. Saravanos, P.R. Heyliger, Coupled layerwise analysis of composite beams with embedded piezoelectric sensors and actuators, *Journal of Intelligent Materials Systems and Structures* 6 (1995) 350–363.

[19] S. Kapuria, An efficient coupled theory for multi-layered beams with embedded piezoelectric sensory and active layers, *International Journal of Solids and Structures* 38 (2001) 9179–9199.

[20] S. Kapuria, P.C. Dumir, A. Ahmed, An efficient coupled layerwise theory for dynamic analysis of piezoelectric composite beams, *Journal of Sound and Vibration* 261 (2003) 927–944.

[21] S. Kapuria, P.C. Dumir, A. Ahmed, An efficient coupled layerwise theory for static analysis of piezoelectric sandwich beams, *Archive of Applied Mechanics* 73 (2003) 147–159.

[22] B.A. Auld, *Acoustic Fields and Waves in Solids*, Vol. I, Wiley, New York, 1973.

[23] A.K. Noor, W.S. Burton, Three-dimensional solutions for initially stressed structural sandwiches, *ASCE Journal of Engineering Mechanics* 120 (1994) 284–303.
[24] M. Cho, R.R. Parmerter, Efficient higher order composite plate theory for general lamination configurations, *American Institute of Aeronautics and Astronautics Journal* 31 (1993) 1299–1306.
[25] H.F. Tiersten, *Linear Piezoelectric Plate Vibrations*, Plenum, New York, 1969.
[26] K. Xu, A.K. Noor, Y.Y. Tang, Three-dimensional solutions for coupled thermoelectroelastic response of multilayered plates, *Computer Methods in Applied Mechanics and Engineering* 126 (1995) 355–371.
[27] R.C. Averril, Y.C. Yip, An efficient thick beam theory and finite element model with zig-zag sublaminate approximation, *American Institute of Aeronautics and Astronautics Journal* 34 (1996) 1626–1632.
[28] S. Kapuria, P.C. Dumir, Coupled FSDT for piezothermoelastic hybrid rectangular plate, *International Journal of Solids and Structures* 37 (2000) 6131–6153.